Microstructure-based modelling of chloride diffusivity in non-saturated cement paste accounting for capillary and gel pores

Cheng Liu [a, b], Mingzhong Zhang [b, *]

[a] Jiangsu Key Laboratory for Construction Materials, School of Materials Science and Engineering, Southeast University, Nanjing 211189, China

[b] Department of Civil, Environmental and Geomatic Engineering, University College London, London WC1E 6BT, UK

Abstract: Accurate prediction of chloride diffusivity in non-saturated cement paste is crucial for durability design of concrete. This paper presents an integrated framework for modelling chloride diffusivity in non-saturated cement paste considering 3D microstructure, water-gas distribution in pore network and electrical double layer effect. Results indicate that the chloride diffusivity in C-S-H pore solution is dominantly influenced by surface electric potential regardless of water saturation level, porosity of C-S-H and chloride concentration of bulk solution. With the decrease of water saturation level, the relative chloride diffusivity in cement paste experiences sharp, slow and slight decrease stages, followed by a non-diffusive stage, corresponding to connected capillary water, combination of capillary water and saturated C-S-H network and non-saturated C-S-H network as the main diffusion channel, and pore depercolation. The relative chloride diffusivity in cement paste at a given water content decreases with increasing water-to-cement ratio. The simulation results show good agreement with experimental data.

Keywords: Microstructure; Pore solution; Electric potential; Moisture distribution; Lattice Boltzmann method

1. Introduction

Concrete is a complex composite material consisting of aggregate, void, and porous matrix formed by the hydration of cementitious materials including Portland cement and supplementary cementitious materials. Owing to the porous nature, the aggressive species from the environment, e.g. ions, oxygen, and water, can transport into concrete via cement paste, leading to the degradation of concrete. Transport properties are normally regarded as important indicators of concrete durability, which directly govern the ingress of aggressive species. Among them, chloride diffusivity is the most critical parameter for assessment of durability and prediction of service life of reinforced concrete structures [1]. In the laboratory, chloride diffusivity of cementitious materials is usually measured at a saturated state while the concrete structures in practice are seldomly saturated due to self-desiccation and change in moisture of service environments and the chloride diffusion is highly dependent on the moisture conditions in concrete in terms of water content and moisture distribution

---

[2]. Therefore, it is vital and significant to investigate the chloride diffusion in partially saturated cementitious materials.

To measure the chloride diffusivity in partially saturated cementitious materials, natural diffusion tests or electrical resistivity tests are generally carried out on the cementitious specimens preconditioned to a certain non-saturated state that is often indicated by degree of water saturation or internal relative humidity (RH) [3]. Regarding natural diffusion tests, the natural process of chloride diffusion is driven by an chloride concentration difference and the chloride diffusivity of cementitious specimens at various non-saturated states can be determined by fitting the measured chloride concentration profile to the solution of Fick's second law of diffusion. The natural diffusion tests have been widely applied to measure the chloride diffusivity in Portland and blended cementitious materials [4-8], which shows a high dependence on the water saturation level. Nevertheless, natural diffusion tests are very time-consuming, which take several months or even years for the specimens with a low degree of water saturation. Besides, it is very difficult to maintain the desired water saturation level in specimens during the whole testing process. To shorten the testing period, the electrical resistivity tests that relate the conductivity of a porous medium to its effective chloride diffusivity using Nernst-Einstein equation were employed to measure the chloride diffusivity in cementitious materials. For instance, Olsson et al. [9, 10] used the electrical resistivity test to measure the chloride diffusivity in non-saturated Portland cement mortar and binary blended cement mortars with slag or silica fume. They found that the relationship between the relative chloride diffusivity that is defined as the ratio of chloride diffusivity at a given non-saturated state over that at the saturated state, and degree of water saturation is not significantly affected by water-to-binder (w/b) ratio. Following a similar procedure, Zhang et al. [11, 12] experimentally studied the chloride diffusivity in mortars with different pore structures and concluded that the effect of pore structure on the relative chloride diffusivity as a function of degree of water saturation results from its effect on water continuity. However, the application of the electrical resistivity method to characterising the chloride diffusivity in cementitious materials is still questionable. Due to the presence of electrical double layer (EDL) induced by the nano-sized pores [13], the chloride diffusivity obtained from the electrical resistivity tests cannot fully represent the realistic diffusion property of cementitious materials. Moreover, for electrical resistivity tests, the attributes of solution in pores are assumed to be the same as those in bulk solution (free water), which is too ideal as the pore solution attributes are highly dependent on the pore structure in reality [14].

In addition to experimental work, analytical and numerical approaches were also proposed to predict the chloride diffusivity in non-saturated cementitious materials over the past decades. For example, Saetta et al. [15] and Baroghel-Bouny et al. [16] respectively established the empirical equations of relative chloride diffusivity as a function of RH or degree of water saturation through

fitting the experimental data, however, the application of these equations is limited to certain conditions (e.g., mortars in lab conditions with wetting by a salt solution after drying or wick action) and the fitting parameters still need to be optimised. Zhang and Ye [17] proposed an analytical model for estimating the relative chloride diffusivity in non-saturated cementitious materials with different pore structures according to the chloride diffusivity at the saturated state, degree of water saturation, and average pore diameter of paste matrix obtained from mercury intrusion porosimetry (MIP) measurements. Nevertheless, the used pore structure in this analytical model is over-simplified and the pore size employed is still suspicious due to the presence of ink-bottle effect and certain assumptions for MIP tests [18]. Furthermore, this model is established based on the Nernst-Einstein equation, which is likely to be not suitable for the pore network of cementitious materials due to the EDL effect. Zhang et al. [19] proposed a lattice Boltzmann (LB) model for numerically simulating the water-gas distribution in capillary pore structure and chloride diffusivity of virtual cement paste simulated by HYMOSTRUC3D [20], where the contribution of gel pores to chloride diffusion in cement paste was not considered. It has been demonstrated that the contribution of gel pores to the water saturation and chloride diffusion process of cementitious materials is significant and cannot be ignored, especially for the situation that the depercolation of capillary pore is approaching [21-23]. Additionally, the effect of EDL on chloride diffusion in the nano-sized pore structure of cement paste was not taken into account.

To this end, the main purpose of this study is to develop an integrated framework for modelling the chloride diffusivity in non-saturated cement paste accounting for the effects of gel pores and EDL on chloride diffusion. First, to represent the hierarchical pore network, the 3D microstructures of calcium silicate hydrate (C-S-H) and cement paste were simulated using the hardcore-softshell (HCSS) algorithm and CEMHYD3D model, respectively. The average chloride diffusivity in pore solution in partially saturated C-S-H gels was analytically estimated using the classical EDL theory. Afterwards, LB multiphase model and LB model for diffusion were proposed to respectively simulate the solid-fluid (water and gas) interaction and equilibrium distribution of water and gas phases in capillary and gel pore networks, and the chloride diffusivity in cement paste with water-to-cement (w/c) ratios of 0.4, 0.5 and 0.6 at various saturation levels. The simulation results of chloride diffusivity in partially saturated cement paste were compared with the experimental data obtained from literature to explore the underlying mechanisms of chloride diffusion in cement paste with various water saturation levels.

2. Modelling of 3D microstructure

Due to the hierarchical nature for the pore structure of cementitious materials, it is impossible to simulate the heterogeneous microstructure of cement paste with all range of pore size at one size-scale considering current computational capacity. Moreover, the cement paste matrix manifests its

heterogeneity at different levels including C-S-H and cement paste. Thus, in this study, the 3D representative volume elements (RVEs) at C-S-H level and cement paste level were simulated following a similar procedure adopted by Ulm et al. [24], Hlobil et al. [25], and Liu et al. [26], which are described in detail below.

2.1. C-S-H level

Based on the colloidal model proposed by Jennings [27] and overlapped C-S-H particles observed from atomic force microscope images [28], the microstructure of C-S-H was reconstructed in this study using the HCSS algorithm [29], where the individual C-S-H particle is assumed to be a sphere with a diameter of 5 nm consisting of an impenetrable hardcore surrounded by a concentric softshell and the ratio of the diameter of hardcore and the thickness of softshell is kept as 3:1, as suggested and adopted in Refs. [28-33]. Regarding the packing criterion, the new softshell can overlap arbitrarily with the existing softshells and hardcores, while the new hardcore can only overlap with the existing softshells. The desired porosity of packing was set as 28%, corresponding to the C-S-H gel formed in hardened Portland cement paste at room temperature [30]. To investigate the effect of porosity of C-S-H gel on chloride diffusion, the other typical porosity of C-S-H gel for blended cement system, i.e., 19% [31], was also taken into consideration. Using the same pre-defined parameters suggested by Liu et al. [32] and Babaei et al. [33], the RVE size of C-S-H was regarded to be $100 \times 100 \times 100$ nm^3 with a resolution of 0.5 nm/voxel. Fig. 1 shows the microstructure of C-S-Hs and pore size distribution of C-S-Hs calculated using the largest sphere method [34]. It can be seen that the pore size of C-S-H is between 1 nm and 6 nm, which is comparable to that reported in Ref. [35], i.e. ranging from 2.5 nm to 5 nm. The simulated pore size distribution in the RVE of C-S-H is shown in Fig. 1c in comparison with that reported by Liu et al. [32] and Babaei et al. [33]. As expected, the simulated pore size in this study is consistently greater than that presented in Refs. [32, 33], where the RVE of C-S-H was simulated using the rigid particle packing model based on the assumption that C-S-H particles cannot overlap with each other during the packing, resulting in a pore network with a smaller size compared to that simulated using the HCSS algorithm.
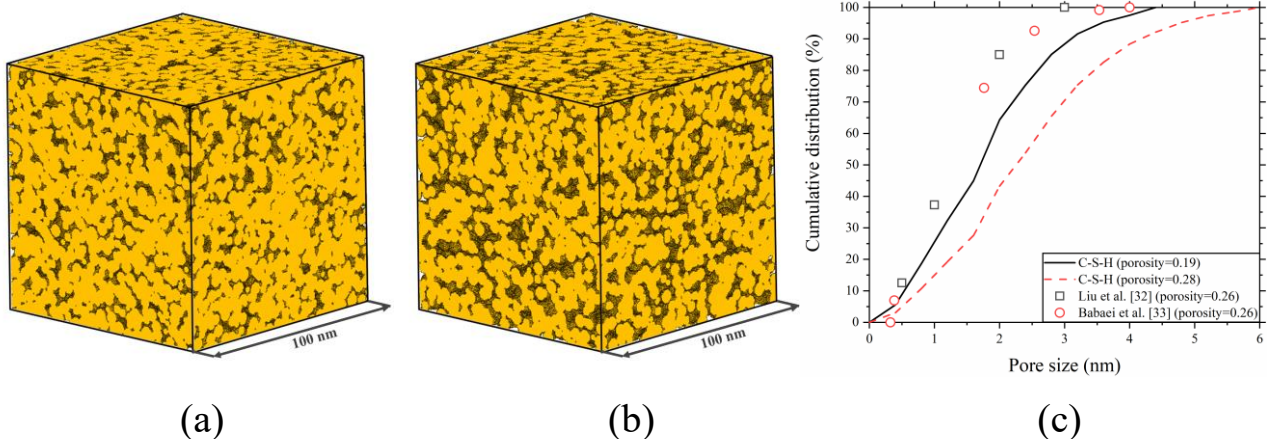

| (a) | (b) | (c) |

Fig. 1. Reconstructed C-S-Hs (yellow – C-S-H particle) with porosities of 0.19 (a) and 0.28 (b); and

(c) pore size distribution simulated in this study against Liu et al. [32] and Babaei et al. [33].

2.2. Cement paste level

The 3D microstructure of hydrating Portland cement paste was simulated using a modified version of CEMHYD3D model [36], which consists of three main steps, i.e. particle packing, phase segmentation, and hydration. First, the cement particles are regarded as digital spheres and randomly packed in a cubic box with size of $200 \times 200 \times 200$ μm^3 and a resolution of 1 μm/voxel according to the particle size distribution and w/c ratio. Subsequently, each cement particle is then segmented into four mineral phases, i.e. tricalcium silicate (C_3S), dicalcium silicate (C_2S), tricalcium aluminate (C_3A), and tetracalcium aluminoferrite (C_4AF), based on the bulk phase composition and auto-correlation functions of the mineral phases. Afterwards, the cellular automaton-like evolution rules with pre-defined dissolution and reaction probabilities are employed to manipulate the movement and phase transition of basic voxels accounting for the reactions in the system, which simulates the cement hydration process and leads to the microstructural development. More details about the modelling procedure and raw material attributes can be found in a previous publication [36]. Fig. 2 displays the simulated 3D microstructure and capillary pore structure of cement paste with w/c = 0.5 at 28 d. Note that the pre-set parameters regarding the RVE size and resolution as well as the cement particle shape can be altered [37]. The pre-set parameters used in this study were selected considering the computation efficiency and accuracy as per the findings shown in Refs. [38-40], where the effects of these pre-set variables on the chloride diffusivity in saturated cement paste were investigated and discussed in detail.

(a)   (b)
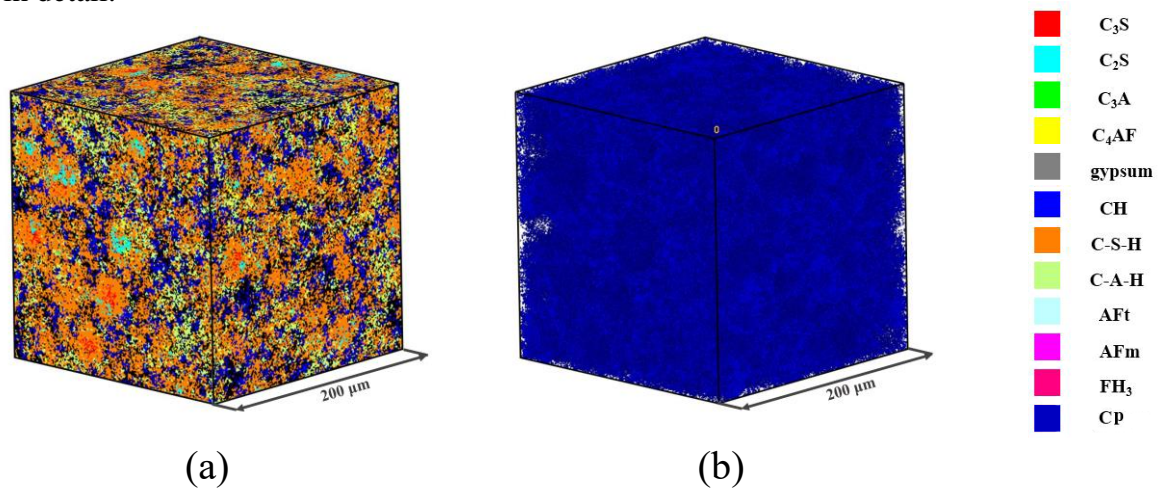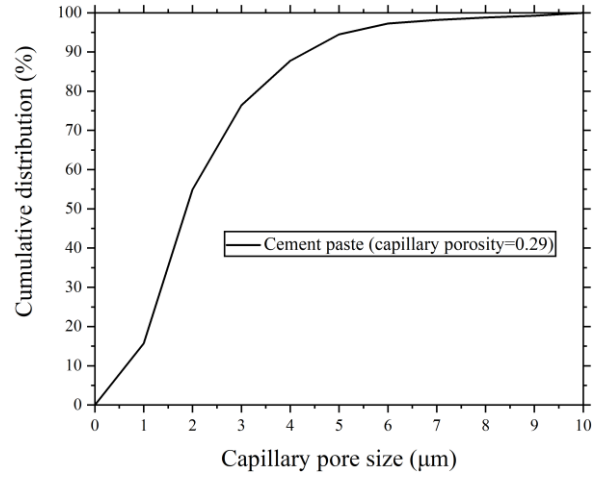
(c)

Fig. 2. Microstructure (a), capillary pore network (b), and capillary pore size distribution (c) of cement paste with w/c = 0.5 at 28 d.

3. Lattice Boltzmann simulation

Herein, two LB models including multiphase LB model and LB model for diffusion were developed to simulate the solid-fluid (water and gas) interaction and water-gas equilibrium distribution in pore network and the chloride diffusion in hydrating cement paste, respectively.

3.1. Multiphase lattice Boltzmann model

To estimate the chloride diffusivity in non-saturated cement paste, it is necessary to simulate the equilibrium distribution of water and gas phases in 3D microstructures of C-S-H and cement paste. Over the past decades, different multiphase LB models have been developed to simulate the multiphase flow in porous media, including colour-gradient model [41], free-energy model [42], phase-field model [43, 44], and pseudopotential multiphase model [45, 46], among which the pseudopotential multiphase model is the most widely used one due to its capability for simulating the multiphase flows with a large density ratio (liquid/gas density ratio of over 1000) as well as its easy implementation and computational efficiency. Therefore, the pseudopotential multiphase LB model was employed in this study, the theory and implementation of which are briefly described below.

3.1.1. Theory

With the Bhantagar-Gross-Krock collision operator, the lattice Boltzmann equation can be represented using the following particle distribution functions:

$$f_i(\mathbf{x} + c\boldsymbol{e}_i\delta t, t + \delta t) - f_i(\mathbf{x}, t) = -\frac{1}{\tau}\left[f_i(\mathbf{x}, t) - f_i^{eq}(\mathbf{x}, t)\right] \tag{1}$$

where f_i and f_i^{eq} are the non-equilibrium and equilibrium particle distribution functions at position $\mathbf{x}$ and time t, c is the lattice speed that is equal to $\delta x/\delta t$, δx is the grid spacing, δt is the time step, $\boldsymbol{e}_i$ is the microscopic velocity at position $\mathbf{x}$ and time t, τ is the relaxation time related to the kinematic viscosity as $\upsilon = c_s^2(\tau - 0.5)\delta t$ with $c_s = c/\sqrt{3}$ where the lattice sound speed c_s is a constant only

6

dependent on the selection of the lattice spacing and time step ($\delta x = 1$ and $\delta t = 1$ in this study), and the subscript $i = 0, 1, \ldots (b - 1)$ denotes the velocity direction where b is the number of the discrete lattice velocity directions.

Herein, the widely used D3Q19 lattice model was selected, which can be expressed as:

$$\mathbf{e}_i =$$
$$\begin{bmatrix} 0 & 1 & -1 & 0 & 0 & 0 & 0 & 1 & 1 & 1 & 1 & 0 & 0 & -1 & -1 & -1 & -1 & 0 & 0 \\ 0 & 0 & 0 & 1 & -1 & 0 & 0 & 1 & -1 & 0 & 0 & 1 & 1 & 1 & -1 & 0 & 0 & -1 & -1 \\ 0 & 0 & 0 & 0 & 0 & 1 & -1 & 0 & 0 & 1 & -1 & 1 & -1 & 0 & 0 & 1 & -1 & 1 & -1 \end{bmatrix} (2)$$

Accordingly, the equilibrium distribution function for the D3Q19 lattice model can be given by:

$$f_i^{eq} = \omega_i \rho \left[1 + \frac{3}{c^2} (\mathbf{e}_i \cdot \mathbf{u}^{eq}) + \frac{9}{2c^4} (\mathbf{e}_i \cdot \mathbf{u}^{eq})^2 - \frac{3}{2c^2} (\mathbf{u}^{eq})^2 \right] \tag{3}$$

where ρ is the macroscopic fluid density, $\mathbf{u}^{eq}$ is the macroscopic fluid equilibrium velocity, and ω_i is the lattice weighing factor that can be expressed as:

$$\omega_i = \begin{cases} \frac{1}{3} & i = 0 \\ \frac{1}{18} & i = 1,2,\ldots,6 \\ \frac{1}{36} & i = 7,8,\ldots,18 \end{cases} \tag{4}$$

The macroscopic fluid density and momentum can be calculated as:

$$\rho = \sum_{i=0}^{18} f_i \tag{5}$$

$$\rho \mathbf{u} = \sum_{i=0}^{18} (f_i \cdot \mathbf{e}_i) \tag{6}$$

The macroscopic fluid equilibrium velocity used in Eq. (3) is given by:

$$\mathbf{u}^{eq} = \mathbf{u} + \frac{\tau \cdot (F_{int} + F_{ads} + F_b)}{\rho} \tag{7}$$

where F_{int} is the fluid-fluid interaction force, F_{ads} is the fluid-solid adhesion force, and F_g is the body force that is generally neglected.

The phase separation results from the cohesive force between liquid particles, i.e. fluid-fluid interaction force F_{int}, which can be described as:

$$F_{int} = -G\psi(\mathbf{x}, t) \sum_{i=0}^{18} \omega_i \psi(\mathbf{x} + \mathbf{e}_i, t) \mathbf{e}_i \tag{8}$$

where G is the coefficient of attractive forces between fluid particles representing the intensity of interparticle interaction, and ψ is the effective mass that is a function of local fluid density ρ.

G is negative for the attraction and positive for the repulsion between particles. The increasing G within the critical value can lead to a tendency to phase separation and a sharper interface. The effective mass function ψ directly relates to the interaction force. The form of ψ controls the detailed nature of the interaction potential and determines the equation of state (EOS) of the fluid system. The effective mass ψ can be expressed as:

$$\psi(\rho) = \sqrt{\frac{2(p - c_s^2 \rho)}{c_s^2 g}} \tag{9}$$

To simulate the multiphase flow with a large density ratio, the following Carnahan-Starling EOS [47] can be introduced and incorporated into Eq. (9):

$$p = \rho R_0 T \frac{1 + \frac{b\rho}{4} + (\frac{b\rho}{4})^2 - (\frac{b\rho}{4})^3}{(1 - \frac{b\rho}{4})^3} - a\rho^2 \tag{10}$$

$$a = 0.4963 R^2 T_c^2 / P_c \tag{11}$$

$$b = 0.18727 R T_c / P_c. \tag{12}$$

where a, b and R are set as 1, 4 and 1 in the simulation, T is the absolute temperature of the gas, T_c is the critical temperature, and P_c is the critical pressure.

Then fluid-solid adhesion force F_{ads} can be expressed as:

$$F_{ads} = -G\psi(\mathbf{x}, t) \sum_{i=0}^{18} \omega_i \psi(\rho_w) s(\mathbf{x} + \mathbf{e}_i)\mathbf{e}_i \tag{13}$$

where ρ_w is the density of solid phase that can be freely adjusted for achieving different contact angles at the interface between fluid and solid phases, and s is an indicator function for checking the neighbouring solid-phase site $(\mathbf{x} + \mathbf{e}_i)$ (1 for solid phase and 0 for liquid or gas phase).

3.1.2. Model implementation

To simulate the equilibrium distribution of water and gas phases in cement paste with various water saturation levels, the pore voxels are randomly transferred into liquid and gas voxels according to the pre-set degree of water saturation. Subsequently, the parameters, e.g., T and ρ_w, need to be qualified for achieving the attributes of real water-gas distribution including water/gas density ratio and contact angle of water on the surface of solid phases composed of hydration products and unhydrated cement particles in cement paste. As suggested by Zhang et al. [19], T was set as 0.585 to achieve a liquid/gas density ratio of 0.4152/0.00053 = 783 that is close to a real water/gas density ratio, i.e., 1000/1.29 = 775. Since the contact angle of water on the surface of cementitious materials is normally regarded as 0° [48], the virtual density of solid phase ρ_w was thus set to be close to the liquid density in lattice units. More details about the modelling of equilibrium water-gas distribution can be found in a previous study [19].

The multiphase LB modelling procedure including streaming and collision steps was then carried out on the porous cement paste with liquid/gas phases. In the simulations, the periodic boundary conditions were imposed on the six surfaces of the RVE of cement paste, while the half-way bounce-back boundary condition was applied to the interface between solid and fluid nodes [49]. Once the relative difference of macroscopic liquid density in the system between time step t and $(t + 1000)$ is $\leq 10^{-5}$ or the time step t reaches 100,000, the equilibrium state was assumed to be achieved, which was also adopted and validated in a previous study [19] through a series of benchmark tests, i.e., bubble tests and contact angle tests. After obtaining the equilibrium state of liquid/gas distribution, the C-S-H in cement paste was converted into a two-phase domain consisting of liquid phase and non-diffusive phase including gas and solid phases, while the 3D microstructure of cement paste was

converted into a three-phase domain composed of liquid phase, C-S-H and non-diffusive phase.

3.2. Lattice Boltzmann model for diffusion

After obtaining the equilibrium water-gas distribution in cement paste with various saturation levels, the chloride diffusivity in cement paste was simulated using a LB model for diffusion [36], where the evolution of particle distribution functions for the pure diffusion is also satisfied with Eq. (1) and $f_i^{eq}(\mathbf{x}, t)$ can be expressed as:

$$f_i^{eq}(\mathbf{x}, t) = \frac{1}{b} C(\mathbf{x}, t) \tag{14}$$

where $C(\mathbf{x}, t)$ is the chloride concentration accounting for the number of particles, i.e. $C(\mathbf{x}, t) = \sum_i f_i(\mathbf{x}, t)$.

It has been indicated that the D3Q7 lattice model can be used instead of D3Q19 to increase the computational efficiency and reduce the computational cost when simulating the pure diffusion process in porous media [50]. The lattice velocity of D3Q7 model can be described as:

$$\mathbf{e}_i = \begin{bmatrix} 0 & 1 & -1 & 0 & 0 & 0 & 0 \\ 0 & 0 & 0 & 1 & -1 & 0 & 0 \\ 0 & 0 & 0 & 0 & 0 & 1 & -1 \end{bmatrix} \tag{15}$$

The non-dimensional relaxation time (τ) for the pure diffusion using D3Q7 lattice model is associated with the chloride diffusivity in lattice units ($\widetilde{D}$) as:

$$\widetilde{D} = \frac{2}{7}\left(\tau - \frac{1}{2}\right) c^2 \delta t \tag{16}$$

where the lattice speed $c = \delta x / \delta t$ ($\delta t = 1$ and $\delta x = 1$) is set as 1 by default.

Thus, cement paste can be treated as a medium with two diffusive phases including C-S-H and water-filled capillary pore, as they both have contributions to the chloride diffusion in cement paste. The relationship between τ and $\widetilde{D}$ for different diffusive phases in the domain can be described as:

$$\frac{\widetilde{D}_1}{\widetilde{D}_2} = \frac{D_1}{D_2} = \frac{\tau_1 - \frac{1}{2}}{\tau_2 - \frac{1}{2}} \tag{17}$$

where $\widetilde{D}_1$ and $\widetilde{D}_2$ are the diffusivity values for diffusive phases 1 and 2 in lattice units ($\widetilde{D}_2 > \widetilde{D}_1$), D_1 and D_2 denote the diffusivity values for diffusive phases 1 and 2 in physical units, and τ_1 and τ_2 represent the relaxation time for diffusive phases 1 and 2, respectively.

Regarding boundary conditions, the inlet/outlet boundary condition is applied at the inlet and outlet of the computational domain, while a solid wall is added for the other four surfaces to ensure there is no diffusive flux through each of them [51]. The periodic condition is applied in the direction corresponding to the concentration gradient so that the nodes on inlet and outlet boundaries are considered as neighbours. At the interface of diffusive and non-diffusive nodes inside the computational domain, the no-ship condition is imposed following the half-way bounce-back rule.

In the simulations, the steady-state diffusion criterion is defined as the convergence of the average chloride concentration at two consecutive time steps $\leq 10^{-8}$ within the whole domain. Once the

steady-state diffusion is achieved, the diffusive flux across the porous medium ($\tilde{J}$) can be calculated from the particle distribution function as:

$$\tilde{J} = \sum_i \mathbf{e}_i f_i \frac{\tau_\alpha - 0.5}{\tau_\alpha} \tag{18}$$

where τ_α represents the relaxation time of diffusive phase α in the porous medium.

The chloride diffusivity of the medium in physical units (D_e) can be subsequently calculated by [36]:

$$\frac{D_e}{D_0} = \frac{\tilde{D}_e}{\tilde{D}_0} = \frac{\tilde{J}}{\tilde{J}_0} \tag{19}$$

where D_0 is the chloride diffusivity in pore solution in physical units, $\tilde{D}_e$ is the effective diffusivity of the porous medium in lattice units, $\tilde{D}_0$ is the chloride diffusivity in pore solution in lattice units, and $\tilde{J}_0$ is diffusive flux across a water-saturated pore space with the same size as the porous medium.

4. Chloride diffusivity in pore solution considering electrical double layer effect

4.1. Electrical double layer

Since the pore size in cementitious materials is hierarchical, ranging from nanometres to micrometres, the effect of EDL on the chloride diffusion should be taken into account [13]. The formation of EDL in cementitious materials can be attributed to the alkalis dissociation and surface silanol groups ionization on the C-S-H surface when in contact with pore solution [52], leading to the negatively charged surface. A small number of cations are strongly absorbed by the C-S-H surface to partially balance the negative charges and thus the remaining negative charges on the surface redistribute the ions in the pore solution, which results in the non-uniform distribution of ions near the surface. The EDL effect in the pore solution of cementitious materials is illustrated in Fig. 3 as per the Stern model [14, 53], where the region of pore solution can be divided into the immobile fluid adhering to the charged surface, i.e. Stern layer, and the mobile fluid including diffuse layer and bulk solution by Stern plane. It is worth noting that the ions in the Stern layer cannot move due to the strong electric attraction, while those in the diffuse layer and bulk solution are freely moveable. The electric potential on the Stern layer is called surface electric potential ($\delta\psi_0$) and is normally replaced by that on the shear plane, i.e. zeta potential, which can be experimentally determined. As a result of the chloride redistribution from the EDL effect, the chloride diffusivity in pore solution of cementitious materials is different from that in bulk solution. An analytical model was proposed to estimate the average chloride diffusivity in pore solution of hydrating cement paste considering the EDL effect, which is introduced in detail below.

4.2. Chloride diffusivity in pore solution of a saturated pore channel

Based on the Poisson-Boltzmann equation [54], the local electric potential, $\delta\psi$, perpendicular to the C-S-H surface (see Fig. 3) can be described as:

$$\frac{\partial^2 \delta\psi_+}{\partial \delta x_+^2} = \sinh \delta\psi_+ \tag{20}$$

$$\delta\psi_+ = \frac{F}{RT}\delta\psi \tag{21}$$

$$x_+ = \kappa x = x\sqrt{\frac{2F^2 C_b}{RT\varepsilon}} \tag{22}$$

where $\delta\psi_+$ is the dimensionless electric potential, x_+ is the dimensionless length, F is the Faraday constant that is equal to 96,485 C·mol^{-1}, R is the gas constant that is equal to 8.314 J·mol^{-1}·K^{-1}, T is the thermodynamic temperature that is set as 298 K in this study, κ is the Debye constant, $1/\kappa$ is the extended length of the diffuse layer, C_b is the ionic concentration of bulk solution, and ε is the dielectric constant that is equal to 10^{-9} F/m.

The solution of the Poisson-Boltzmann equation can be expressed as [55]:

$$\delta\psi_+ = 2\ln\left(\frac{1+\tanh\left(\frac{\delta\psi_{+0}}{4}\right)exp(-x_+)}{1-\tanh\left(\frac{\delta\psi_{+0}}{4}\right)exp(-x_+)}\right) \tag{23}$$

When the of ionic distribution in a pore channel is reached, the ionic concentration in the diffuse layer, C_d, can be calculated as:

$$C_d = C_b\,exp(-z\delta\psi_+) \tag{24}$$

where z is the ionic valence.

Combining Eqs. (23) and (24), the concentration of transportable ion, C_{tr}, in the diffuse layer can be deduced as:

$$C_{tr} = C_d = C_b\left(\frac{1+\tanh\left(\frac{\delta\psi_{+0}}{4}\right)exp(-x_+)}{1-\tanh\left(\frac{\delta\psi_{+0}}{4}\right)exp(-x_+)}\right)^{-2z} \tag{25}$$

Given that the diffuse layers may overlap with each other for the nano-sized pore, the dimensionless electric potential can be modified as the sum of electric potential for 0 to diameter d ($\delta\psi_{0\text{-}d}$ plus $\delta\psi_{d\text{-}0}$) [14, 56]:

$$\delta\psi_+ = \delta\psi_{+0-d_+} + \delta\psi_{+d_+-0} = 2\ln\left(\frac{1+\tanh\left(\frac{\delta\psi_{+0}}{4}\right)exp(-x_+)}{1-\tanh\left(\frac{\delta\psi_{+0}}{4}\right)exp(-x_+)}\right) + 2\ln\left(\frac{1+\tanh\left(\frac{\delta\psi_{+0}}{4}\right)exp(-(d_+-x_+))}{1-\tanh\left(\frac{\delta\psi_{+0}}{4}\right)exp(-(d_+-x_+))}\right) \tag{26}$$

where d_+ is the dimensionless pore diameter that is equal to κd.

Correspondingly, the concentration of the transportable ion in overlapping diffuse layers can be described as:

$$C_{tr} = C_b\left(\left(\frac{1+\tanh\left(\frac{\delta\psi_{+0}}{4}\right)exp(-x_+)}{1-\tanh\left(\frac{\delta\psi_{+0}}{4}\right)exp(-x_+)}\right)\left(\frac{1+\tanh\left(\frac{\delta\psi_{+0}}{4}\right)exp(-(d_+-x_+))}{1-\tanh\left(\frac{\delta\psi_{+0}}{4}\right)exp(-(d_+-x_+))}\right)\right)^{-2z} \tag{27}$$

For a saturated pore channel, the average concentration of transportable ion, $\bar{C}_{tr}$, can be deduced as:

$$\bar{C}_{tr} = \frac{C_b \int_0^{d_+} \left(\left(\frac{1+\tanh\left(\frac{\delta\psi_{+0}}{4}\right)exp(-x_+)}{1-\tanh\left(\frac{\delta\psi_{+0}}{4}\right)exp(-x_+)} \right) \left(\frac{1+\tanh\left(\frac{\delta\psi_{+0}}{4}\right)exp(-(d_+-x_+))}{1-\tanh\left(\frac{\delta\psi_{+0}}{4}\right)exp(-(d_+-x_+))} \right) \right)^{-2z} dx_+}{d_+} \tag{28}$$

Defining $\bar{C}_{tr}/C_b$ as N_i, for the steady-state diffusion in a pore channel with a small concentration difference between the inlet and outlet, the ionic diffusivity in pore solution considering the EDL effect ($D_{EDL,p}$) relative to that in bulk solution ($D_b = 2.03 \times 10^{-9}$ m²/s for chloride ion [36]) is equal to $\bar{C}_{tr}/C_b$ and can be expressed as:

$$N_i = \frac{D_{EDL,p}}{D_b} = \frac{\bar{C}_{tr}}{C_b} = \frac{\int_0^{d_+} \left(\left(\frac{1+\tanh\left(\frac{\delta\psi_{+0}}{4}\right)exp(-x_+)}{1-\tanh\left(\frac{\delta\psi_{+0}}{4}\right)exp(-x_+)} \right) \left(\frac{1+\tanh\left(\frac{\delta\psi_{+0}}{4}\right)exp(-(d_+-x_+))}{1-\tanh\left(\frac{\delta\psi_{+0}}{4}\right)exp(-(d_+-x_+))} \right) \right)^{-2z} dx_+}{d_+} \tag{29}$$

This equation can be numerically solved using MATLAB. In this study, taking the chloride ion as an example, the effect of pore size on $D_{EDL,p}/D_b$ with various surface electric potentials (-10 mV, -30 mV and -50 mV) and chloride concentrations of bulk solution (0.1 mol/l and 0.5 mol/l close to that in seawater) is shown in Fig. 4. It can be found that D_{EDL}/D_b is ≤ 1, suggesting that the negatively charged surface can retard the chloride diffusion. This finding is consistent with those obtained from molecular dynamic simulation [57, 58] and electrokinetic simulation [13] that the chloride diffusivity in gel pore channel is smaller than that in bulk solution. Moreover, $D_{EDL,p}/D_b$ is increased with the increase of pore size following a three-stage increasing trend, i.e. a stable stage below 10 nm, a sharp increase stage between 10 nm and 200 nm, and a stable stage close to 1000 nm. The EDL effect becomes more significant for a given sized pore with the increasing surface electric potential or decreasing chloride concentration. However, as the pore size approaches to 1000 nm, $D_{EDL,p}/D_b$ is close to 1, indicating a negligible EDL effect. Since the resolution of digitized microstructure of cement paste is 1 μm/voxel in this study, the nanoscale effect was only considered at C-S-H level but ignored at cement paste level. A similar assumption was applied in Refs. [26, 59], in which the gas Knudsen diffusion and electrokinetic transport in cementitious materials were simulated, respectively.
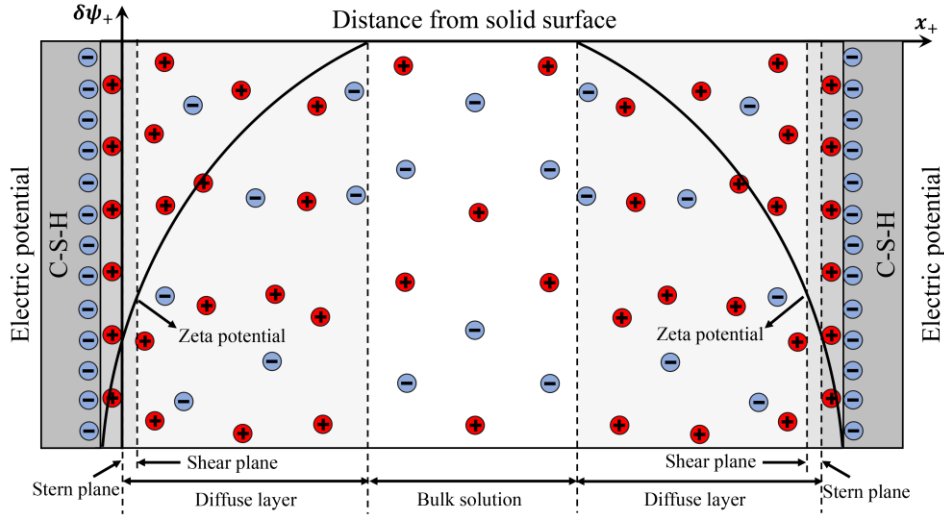
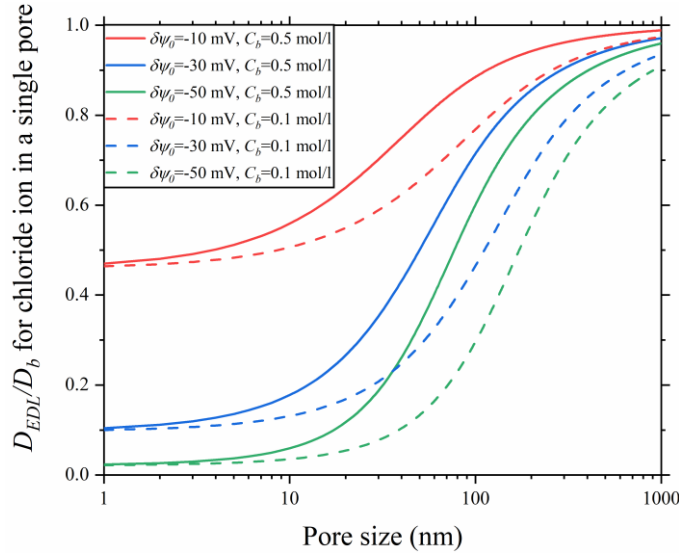Fig. 3. Electrical double layer in a nano-sized pore channel of saturated cementitious materials.

Fig. 4. Effects of surface electric potential and chloride concentration of bulk solution on contrast ratio of chloride diffusivity considering EDL to that in bulk solution as a function of pore size for a pore channel.

4.3. Chloride diffusivity in pore solution in C-S-H

To cover the complex pore network, the effect of EDL on chloride diffusion in pore solution in a saturated porous medium at nano-scale, e.g. C-S-H gel, can be estimated by:

$$\bar{D}_{r,EDL,p} = \frac{\bar{D}_{EDL,p}}{D_b} = \frac{\sum_{i=1}^{n} N_i V_i}{V} \tag{30}$$

where $\bar{D}_{EDL,p}$ ($\bar{D}_{r,EDL,p}$) is the average (relative) chloride diffusivity in pore solution in the saturated porous medium, V_i is the volume fraction of pore with a diameter of d_i, and V is the total volume of pore.

Regarding the non-saturated situation, according to the Kelvin-Laplace equation [60], the water-filled pores in the porous medium at nano-scale are progressively occupied with gas following the sequence from large pores to small pores with the decrease of water saturation level. As a result, the

volume fraction of pore (V_i) in Eq. (30) can be replaced by the normalised volume fraction of water-filled pores in a partially saturated porous medium with a given water saturation level. It should be mentioned that the deformation of small pores in C-S-H gels or contraction of C-S-H gels would occur during drying, leading to a possible change in gel pore network [61-64], which is beyond the scope of this study and thus was not considered. For future research, the moving boundary conditions can be incorporated into the multiphase LB model adopted in this study to account for the changing gel pore structure during drying and rewetting cycles [65]. Based on the pore size distribution of C-S-H shown in Fig. 1c, the effects of surface electric potential, chloride concentration of bulk solution, and C-S-H porosity on the average relative chloride diffusivity in pore solution in C-S-H ($\overline{D}_{r,EDL,p}$), against degree of water saturation are estimated and illustrated in Fig. 5. It can be seen that $\overline{D}_{r,EDL,p}$ is dramatically affected by the surface electric potential. For instance, as the surface electric potential increases form -10 mV to -50 mV, $\overline{D}_{r,EDL,p}$ is decreased from 0.45 to 0.02, equivalent to the chloride diffusivity decreasing from 9.14×10^{-10} m^2/s to 4.06×10^{-11} m^2/s. However, $\overline{D}_{r,EDL,p}$ is insensitive to the degree of water saturation, chloride concentration of bulk solution and porosity of C-S-H, which can be ascribed to the small pore size of C-S-H, i.e. ≤ 10 nm. As seen in Fig. 4, the value of $D_{EDL,p}/D_b$ becomes stable for the pores with size ≤ 10 nm, regardless of chloride concentration of bulk solution.

As discussed above, the surface electric potential is a key parameter for the chloride diffusivity in pore solution in C-S-H. However, the surface electric potential of C-S-H is significantly affected by pore solution [66, 67] in terms of pH value and alkaline cation, and Ca/Si ratio of C-S-H [68], which brings a huge difficulty for determining its quantitative relationship. In this study, the pore solution in C-S-H is simplified to be NaCl monovalent electrolyte solution during the ionic diffusion process [13]. For the low ionic valence electrolyte solution, e.g. NaCl and LiCl, the Zeta potential of C-S-H is not dramatically affected by ionic concentration and ionic type of pore solution [68]. Additionally, the Zeta potential of C-S-H produced from C$_3$S was found to be around -30 mV in the NaCl electrolyte solution with an extremely low calcium concentration, i.e., ≤ 0.1 mmol/l [68, 69]. Thus, -30 mV was used to represent the surface electric potential of C-S-H to investigate the chloride diffusion in C-S-H for Portland cement systems. As the chloride diffusivity in pore solution in C-S-H is insensitive to the degree of water saturation, chloride concentration of bulk solution, and porosity of C-S-H (see Fig. 5), $D_{EDL,p}$ for C-S-H with surface electric potential of -30 mV is accordingly calculated to be 2.03×10^{-10} m^2/s, which is close to 1.07×10^{-10} m^2/s obtained from the inversion analysis on the measured data of chloride diffusivity in cement paste [70]. The chloride diffusivity in capillary pore solution of cement paste is assumed to be the same as that of free water, i.e. 2.03×10^{-9} m^2/s, considering the negligible EDL effect (see Fig. 4).
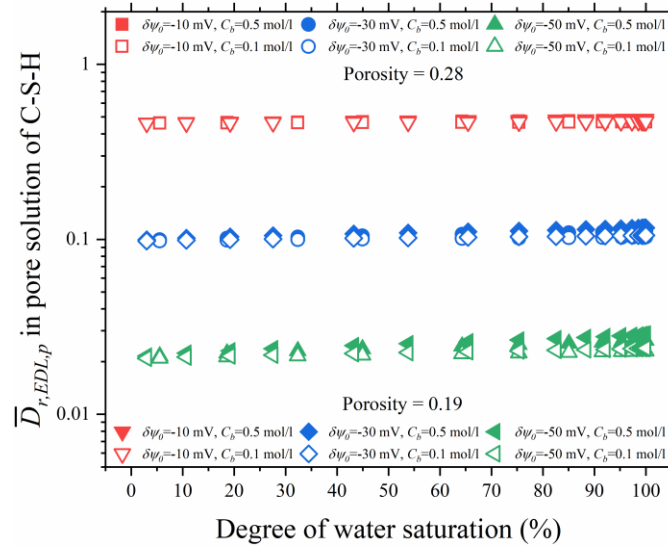
Fig. 5. Effects of surface electric potential and chloride concentration of bulk solution on average relative chloride diffusivity in pore solution in C-S-H as a function of degree of water saturation.

5. Results and discussion

5.1. Chloride diffusivity in C-S-H with various saturation levels

The equilibrium distribution of water and gas phases in C-S-H with various degrees of water saturation can be simulated using the multiphase LB model. Fig. 6a and b show the equilibrium water-gas distribution in the 3D microstructure and gel pore structure of C-S-Hs with degree of water saturation of 63%. It can be found that the water phase tends to cover the solid surface and fill the small pores, while the gas phase tends to form the gas clusters and fill the large pores. This agrees well with the finding obtained from the simulations using the pore geometry method based on the Kelvin-Laplace equation that water is gradually removed from the large pores and then the small pores with the reduction of degree of water saturation [71]. As the water-filled pores are crucial for chloride diffusion, the equilibrium distribution of water in the pore structure of C-S-H gel and connected water-filled pores in C-S-H gel determined using the burning algorithm [72] are shown in Fig. 6c and d. The connectivity (i.e., the ratio of the connected pore volume to the total pore volume) of water-filled pores in C-S-Hs with porosities of 19% and 28% at degree of water saturation of 63% is found to be 0.96 and 0.98, respectively.
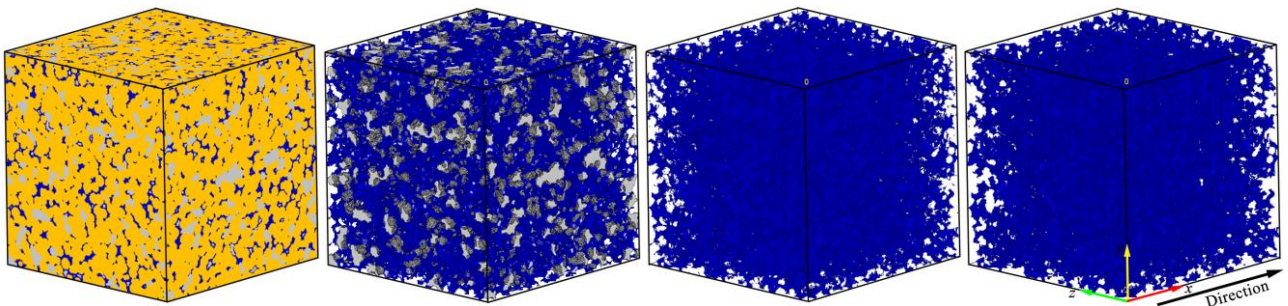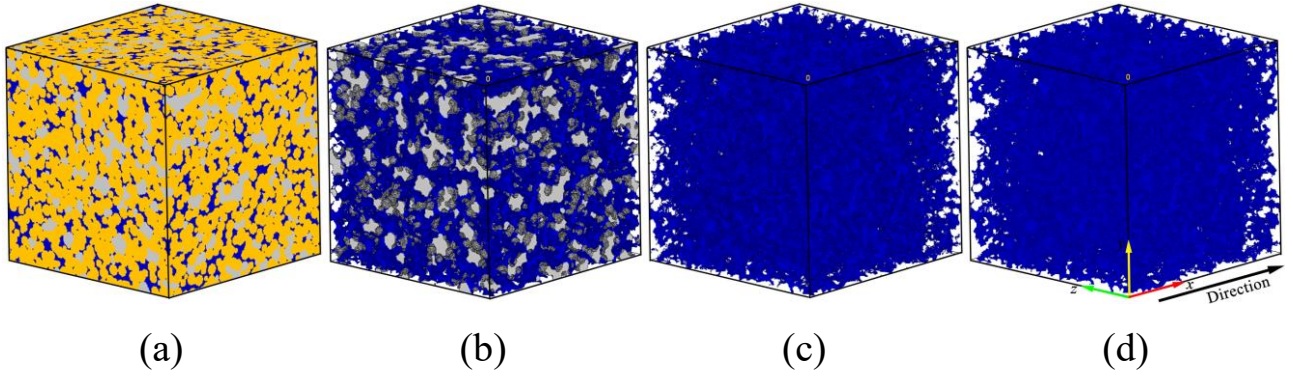
Fig. 6. Equilibrium distribution of water-gas in microstructure (a) and gel pore structure (b), equilibrium distribution of water gel pore structure (c), and connected water-filled gel pores (d) in C-S-Hs with porosities of 0.19 (up) and 0.28 (bottom) at degree of water saturation of 63%; Different colourful voxels represent: grey – gas, blue – water; and yellow – C-S-H solid.

Treating water-filled gel pores as a diffusive phase, the chloride diffusivity in C-S-H at various degrees of water saturation can be simulated using the developed LB model for diffusion. Fig. 7 displays the chloride concentration distribution under the steady-state of diffusion in C-S-Hs at degree of water saturation of 63%. The relative chloride diffusivity in non-saturated C-S-Hs with porosities of 19% and 28% calculated using Eqs. (18) and (19) is shown Fig. 8. Here, the chloride diffusivities in saturated C-S-Hs are calculated to be 7.75×10^{-12} m^2/s and 1.83×10^{-11} m^2/s, respectively. As can be seen, the relative chloride diffusivity is decreased with the reduction of degree of water saturation, which can be attributed to the decreasing effective water-filled porosity as a result of the decreasing water-filled porosity and connectivity of water-filled pores. Additionally, as the degree of water saturation reduces to a critical value, i.e. 24% and 21% for C-S-Hs with porosities of 19% and 28%, the chloride diffusivity becomes zero. The effective water-filled porosity of C-S-H at various degrees of water saturation, i.e. water-filled porosity multiplied by connectivity of water-filled pores (determined using the burning algorithm [72]) in C-S-H gels, is also calculated and displayed in Fig. 8, which indicates that the water-filled gel pores become depercolated at these two critical degrees of water saturation. Regarding the effect of porosity of C-S-H gel, the decreasing tendency of relative chloride diffusivity for C-S-H with porosity of 19% is sharper than that for C-S-H with porosity of 28%, which can be explained by the fact that the decreasing amplitude of effective water-filled porosity of C-S-H with the reduction of degree of water saturation is less significant for the C-S-H with a lower porosity (see Fig. 8). Thus, the relative chloride diffusivity in C-S-H with porosity of 19% is more sensitive to the decrease of water saturation compared to that with porosity of 28%. This is consistent with the finding by Zhang et al. [73] that the denser porous medium exhibited a more significant decreasing tendency of relative chloride diffusivity against water saturation level and a higher critical degree of water saturation.
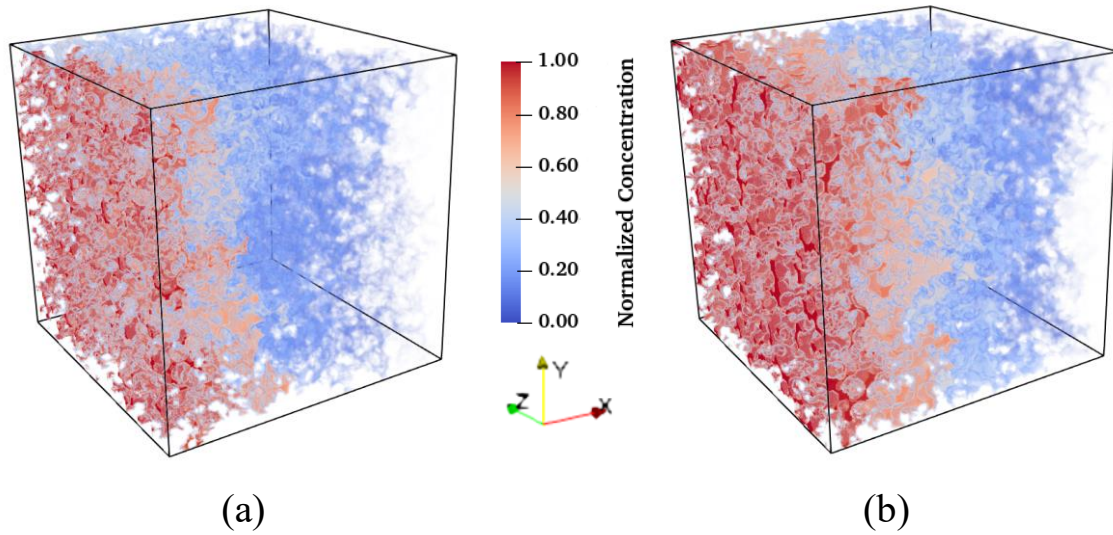
Fig. 7. Steady-state distribution of chloride concentration in C-S-Hs with porosities of 0.19 (a) and 0.28 (b) at degree of water saturation of 63% along *X*-direction.
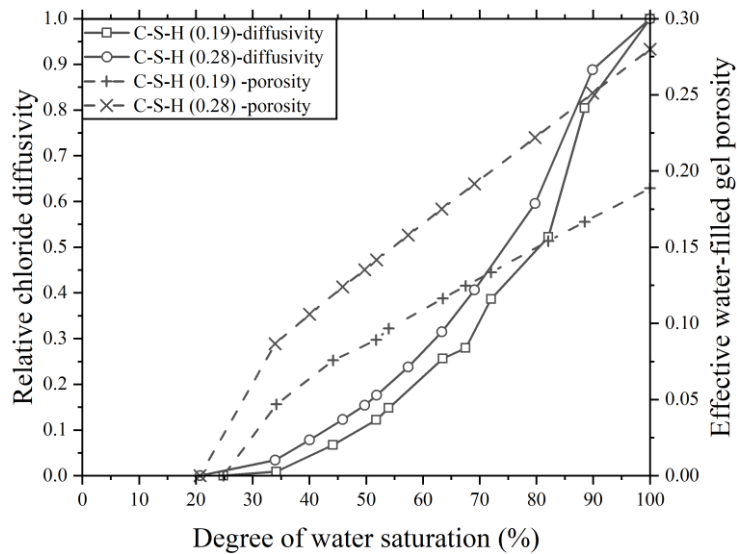

Fig. 8. Relative chloride diffusivity and effective water-filled porosity of C-S-H as a function of degree of water saturation in C-S-H.

5.2. Chloride diffusivity in cement paste with various saturation levels

5.2.1. Effect of degree of water saturation

The chloride diffusivity in non-saturated cement paste can be simulated using the generated 3D microstructure and the chloride diffusivity in C-S-H with porosity of 28% estimated in Section 5.1. Note that the degree of water saturation at cement paste level is made up of water in capillary pores and water in C-S-H gel pores. According to the Kelvin-Laplace law [71], it can be assumed that with the decrease of water saturation level, the water in capillary pores is first removed, followed by the water in C-S-H gel pores. Using the developed multiphase LB model, the solid-fluid interaction in microstructure and capillary pore structure of hydrating cement paste at various degrees of water saturation can be simulated and the corresponding distribution of water and gas phases in capillary pore structure can be obtained once the interaction reaches the equilibrium state. Fig. 9a and b display

17

an example of the equilibrium water-gas distribution in the microstructure and capillary pore network of cement paste with w/c = 0.5 at 28 d (corresponding to that in Fig. 2) at degree of water saturation of 77%, including capillary pore water plus C-S-H pore water content. As can be seen, similar to that observed for C-S-H shown in Fig. 6, the water phase in capillary pore network tends to fill small pores while the gas phase tends to form gas clusters in cement paste. The equilibrium distribution of water in capillary pore network and connected water-filled capillary pores in cement paste at degree of water saturation of 77% are shown in Fig. 9c and d. It can be observed that most of water-filled capillary pores in cement paste are disconnected, the calculated connectivity of which along diffusion direction (X-direction) is only about 0.15. With the obtained equilibrium distribution of water and gas phases in microstructure of cement paste at any given saturation level, the chloride diffusion process and chloride diffusivity in cement paste can be simulated using the developed LB model for diffusion. Fig. 10 shows the steady-state distribution of chloride concentration in cement paste corresponding to the microstructure and moisture distribution illustrated in Fig. 9. The distribution of chloride concentration along diffusion direction is non-uniform due to the presence of two diffusive phases in cement paste, i.e., capillary pores and gel pores in C-S-H, with an obvious difference (around an order of magnitude) in chloride diffusivity in them, as discussed in Section 4.3. Based on the obtained chloride concentration distribution, the total diffusive flux through the outlet plane of 3D microstructure (i.e. RVE) of cement paste can be calculated as well as the corresponding chloride diffusivity according to Fick's law, which is found to be 7.23×10^{-12} m^2/s. Despite the different nature of the materials under study, this calculated value of chloride diffusivity is in fairly good agreement with the experimentally determined chloride diffusivity using Portland cement concrete specimens with w/c ratio of 0.5 conditioned to a water saturation degree of 80%, which was found to be 6.55×10^{-12} m^2/s [7].

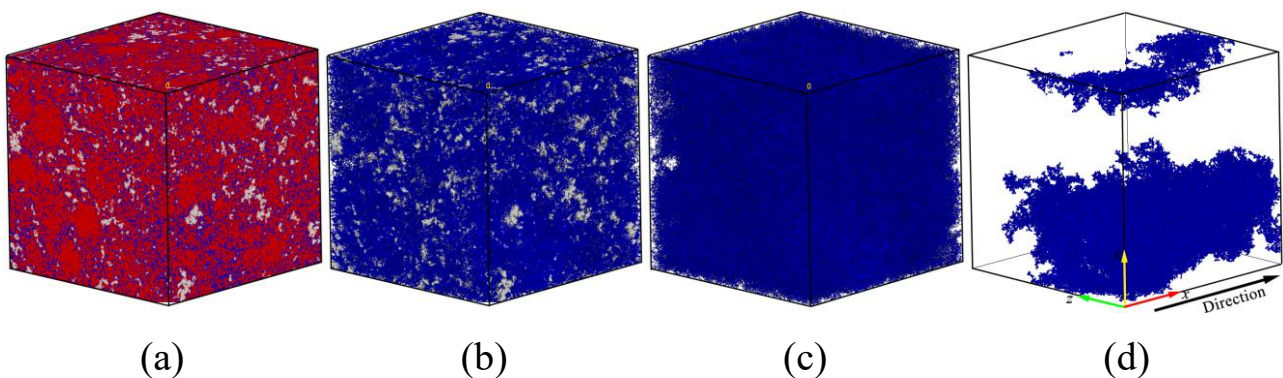| (a) | (b) | (c) | (d) |

Fig. 9. Equilibrium distribution of water-gas in microstructure (a) and capillary pore structure (b), equilibrium distribution of water in capillary pore structure (c), and connected water-filled capillary pores (d) in cement paste with w/c = 0.5 at 28 d and degree of water saturation of 77%; Different colourful voxels represent: grey – gas, blue – water; and red – solid.
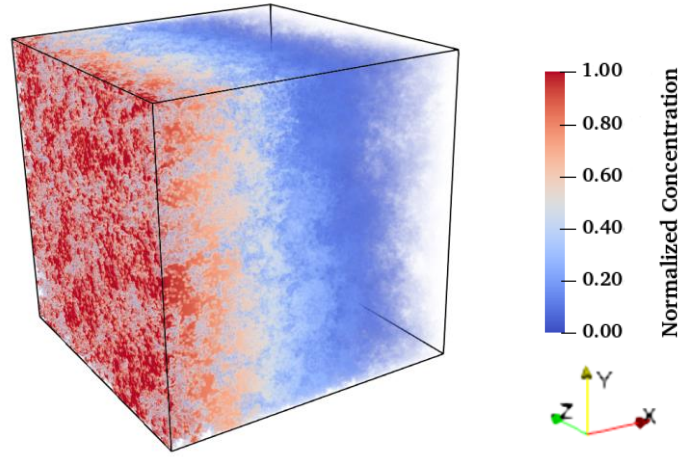
Fig. 10. Steady-state distribution of chloride concentration in cement paste at degree of water saturation of 77% along *X*-direction.

It is worth noting that the connectivity of water-filled capillary pores in cement paste is dependent on the diffusion direction. With the decrease of water-filled capillary porosity, the connectivity of water-filled capillary pores in partially saturated cement paste becomes more sensitive to the diffusion direction due to the low water-filled capillary porosity. For instance, the connectivity of water-filled capillary pores in cement paste at a saturation degree of 77% along *Y*- and *Z*-direction is 0 and 0.20, respectively, as indicated in Fig. 9, while the corresponding chloride diffusivity values are 7.20×10^{-12} m^2/s and 7.25×10^{-12} m^2/s, respectively, which are approximately identical to that along diffusion direction, i.e. *X*-direction. Thus, the simulations for the RVE of cement paste along *X*-direction were carried out solely below.

Fig. 11 shows the effect of degree of water saturation on relative chloride diffusivity in cement paste with w/c = 0.50 at 28 d (circle and line), where the chloride diffusivity in saturated cement paste is 2.23×10^{-11} m^2/s. It can be found that the simulated relative chloride diffusivity in cement paste is strongly dependent on degree of water saturation, the evolution of which can be divided into four stages: (1) A sharp reduction in relative chloride diffusivity from 1.00 to 0.26 with the decrease of water saturation degree from 100% to 72%; (2) A slow decrease of relative chloride diffusivity from 0.26 to 0.07 with decreasing degree of water saturation from 72% to 33%; (3) A further slight drop in relative ionic diffusivity until the degree of water saturation approaches to 8%; (4) Depercolation of pores in cement paste occurs at a water saturation of 8% and the chloride diffusivity becomes zero when the degree of water saturation is ≤ 8% as there is no available connected pore network in cement paste for chloride diffusion.

The change in chloride diffusivity in partially saturated cement paste is strongly related to the equilibrium distribution of water and gas phases in the pore network of cement paste. Due to the relatively higher chloride diffusivity, the water-filled capillary pores play a critical role in chloride diffusion in cement paste [74]. With the decrease of water saturation, the water-filled capillary pores

19

become less, leading to a reduction in effective water-filled capillary porosity. The evolution of effective water-filled capillary porosity in cement paste as a function of degree of water saturation is shown in Fig. 12. With decreasing degree of water saturation from 100% to 72%, the effective water-filled capillary porosity is significantly reduced from 22% to 0, which can be mainly attributed to the decreasing connectivity of water-filled capillary pores from 0.76 to 0. Consequently, a sharp reduction in relative chloride diffusivity can be observed. With a further decrease of water saturation degree from 72%, the water-filled capillary pores tend to be disconnected, i.e., the depercolation of capillary pores happens. At that moment, the water-filled gel pores in C-S-H start playing a crucial role in chloride diffusion together with disconnected water-filled capillary pore network in cement paste to provide available diffusion paths [13], as a result of which there exists only a slow decrease in relative chloride diffusivity in cement paste when the degree of water saturation is reduced from 72% to 33%. As the degree of water saturation reaches 33%, all the capillary pores are occupied by gas phase and only the partially saturated C-S-H network contributes to ionic diffusion in cement paste. Due to the relatively low ionic diffusivity in partially saturated C-S-H gel pores, the decreasing trend of relative chloride diffusivity in cement paste is slight for a degree of water saturation $\leq 33\%$, which is consistent with the critical degree of water saturation experimentally estimated by de Vera et al. [7], corresponding to the minimum liquid content necessary for the existence of a connected path allowing the diffusion of chloride species through a porous material, like Portland cement concrete with w/c ratio of 0.6. With a further decrease of degree of water saturation to 8%, the water-filled gel pores in C-S-H become disconnected and the depercolation of entire pore network takes place, so that there is no available connected pore path for chloride diffusion in cement paste, as seen in the corresponding zero chloride diffusivity in Fig. 12.

As indicated in Section 4.2, the surface electric potential has a significant influence on the chloride diffusivity in pore solution and thus would affect the relative chloride diffusivity in cement paste. To estimate the effect of surface electric potential on relative chloride diffusivity in cement paste at various saturation levels, different values of surface electric potential (-10, -30 and -50 mV) are considered for simulations, the results of which are also illustrated in Fig. 11. The chloride diffusivity in saturated cement paste with w/c = 0.5 and various surface electric potential ranges from 6.57×10^{-11} m^2/s to 7.68×10^{-12} m^2/s. It can be observed that the increasing surface electric potential results in a decrease in relative chloride diffusivity due to the lower chloride diffusivity in C-S-H at a given degree of water saturation. However, the critical degrees of water saturation for dividing the change stages of relative chloride diffusivity are identical for cement paste with same w/c ratio, regardless of surface electric potential.
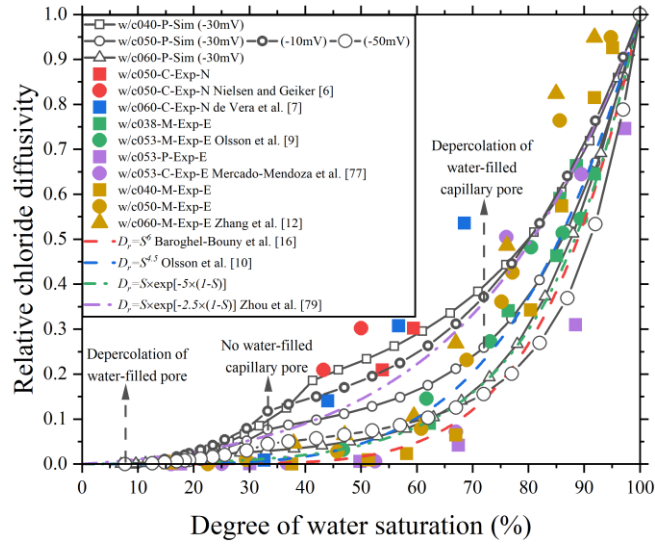
Fig. 11. Relative chloride diffusivity as a function of degree of water saturation in cement pastes with various w/c ratios (Sim – simulation; Exp – experiment; P – paste; M – mortar; C – concrete; N – natural diffusion; E – electrical resistivity).
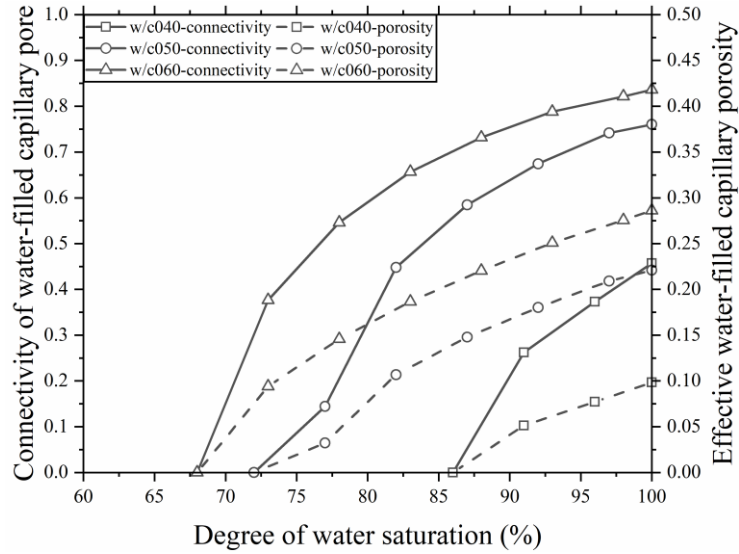

Fig. 12. Connectivity of water-filled capillary pore and effective water-filled capillary porosity as a function of degree of water saturation in cement pastes with various w/c ratios.

5.2.2. Effect of water-to-cement ratio

To investigate the effect of w/c ratio on chloride diffusivity in non-saturated hydrating cement paste, simulations were also carried out on cement paste with w/c ratios of 0.40 and 0.60 at 28 d, in addition to w/c = 0.5. The chloride diffusivity in saturated cement paste with w/c ratios of 0.40 and 0.60 at 28 d is found to be 9.19×10^{-12} m^2/s and 5.46×10^{-11} m^2/s, respectively. The relative chloride diffusivity in cement paste with w/c ratios of 0.4, 0.5 and 0.6 against degree of water saturation is plotted in Fig. 11. It can be seen that the decreasing tendency of relative chloride diffusivity in cement paste with the reduction of water saturation for w/c = 0.40 and 0.60 is similar to that with w/c = 0.50. Nevertheless, for cement paste with a higher w/c ratio, e.g. w/c = 0.60, the sharp drop stage with decreasing degree of water saturation becomes more dramatic, while the following slow decrease

21

stage and slight reduction stage are less significant. Additionally, the critical degrees of water saturation for dividing the evolution of relative chloride diffusivity decrease with the increase of w/c ratio. For example, when the w/c ratio of cement paste increases from 0.5 to 0.6, the critical degrees of water saturation of cement paste are respectively reduced from 72%, 33% and 8% to 68%, 28% and 7%. Moreover, the relative chloride diffusivity in cement paste at a given water saturation level is decreased with the increase of w/c ratio. These findings can be attributed to the different constituents of pore structure in cement paste resulting from different w/c ratios. The increasing w/c ratio can lead to an increase in capillary porosity [75] and connectivity of capillary pores [76]. As shown in Fig. 12, as the w/c ratio increases from 0.40 to 0.60, the connectivity of capillary pores and effective capillary porosity are increased from 0.45 to 0.84 and from 0.10 to 0.29, respectively. This indicates that the role of water-filled capillary pore network in chloride diffusivity becomes more significant for cement paste with a higher w/c ratio. Since the water-filled capillary pore network is the dominant channel for chloride diffusion, the relative chloride diffusivity in cement paste with a higher w/c ratio at the sharp drop stage is thus more sensitive to the decreasing water saturation degree, while those at the slow and slight decrease stages tend to be less significant. Moreover, as the capillary porosity of cement paste is increased with increasing w/c ratio, the effective water-filled capillary porosity is increased at a given non-saturated state (see Fig. 12). Thus, the critical degrees of water saturation are all decreased with the increase of w/c ratio.

5.2.3. Validation of simulations with experimental data

For comparison, the available experimental data of relative chloride diffusivity in partially saturated cementitious materials obtained from literature [6, 7, 9, 12, 77] were plotted together with simulation results in Fig 11. The detailed information on test samples, sample preconditioning and test methods including natural diffusion tests and electrical resistivity tests are summarised in Table 1. It should be noted that only one group of experimental data of cement paste is available in literature, which agree well with the simulation results of cement paste with the surface electric potential of -50 mV (see Fig. 11). Due to the limited experimental data of cement paste, the relative chloride diffusivity in mortar or concrete was also collected for comparison, which was found to be highly associated with the relative chloride diffusivity in cement paste [1, 3, 11]. Buchwald [78] suggested that the relative chloride diffusivity in non-saturated masonry materials can be expressed as an empirical power function of degree of water saturation, which was employed to predict the relative chloride diffusivity in cementitious materials [10]. In addition, Zhou et al. [79] proposed another simple and efficient exponential law for relative chloride diffusivity in cementitious materials. The calculation results from the empirical equations are also presented in Fig. 11. The simulation results show good agreement with experimental data in terms of changing tendency. The simulated chloride diffusivity against degree of water saturation for cement paste with w/c = 0.6 follows a power function and an

exponential function. To further verify the simulations, the relative chloride diffusivity in non-saturated cement paste is expressed as a function of water-filled porosity in Fig. 13. Note that the experimental data of porosity used for comparison is the porosity of cement paste matrix (see Table 1), which was converted and obtained according to the mix proportion of mortar or concrete listed in Refs. [7, 9, 12, 77]. The density of water, Portland cement and aggregate is assumed to be 1.00 g/cm^3, 3.15 g/cm^3 and 2.60 g/cm^3, respectively. The simulated and experimental results [9, 12] both indicate that for cement paste with the same water-filled porosity, the relative chloride diffusivity at various water saturation levels decreases with the increase of w/c ratio and the relative chloride diffusivity in non-saturated cement paste with a higher porosity is more sensitive to the decrease of water content. The values of simulated relative chloride diffusivity in non-saturated cement paste all lie within the range of experimental data.
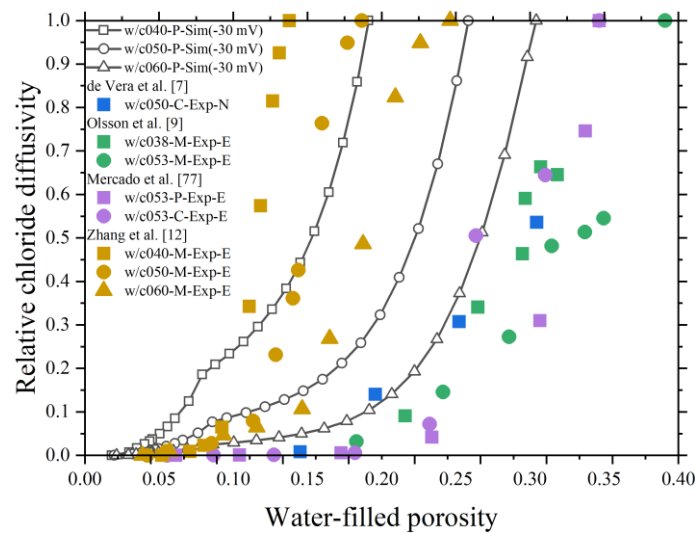

Fig. 13. Relative chloride diffusivity as a function of water-filled porosity in cement pastes with various w/c ratios (Sim – simulation; Exp – experiment; P – paste; M – mortar; C – concrete; N – natural diffusion; E – electrical resistivity).

Although the simulation results agree well with experimental data, some issues and uncertainties regarding the experimental measurements and numerical simulations still need to be clarified and discussed. From an experimental point of view, it is still a big challenge for sample pre-conditioning to achieve a desired degree of water saturation because the water in C-S-H gel pores cannot be completely removed even the sample is conditioned to an extremely low RH [80]. As a result, the measured degree of water saturation from experiments is usually higher than the actual value, which is between capillary saturation (upper limit) and vacuum saturation (low limit). Here, the degree of capillary saturation denotes the ratio between residual capillary water content and fully saturated capillary water content, while the degree of vacuum saturation means the ratio between residual water content including capillary water and gel water, and fully saturated pore water content. Nielsen and Geiker [6] investigated the chloride diffusivity in non-saturated mortar as a function of degree of

capillary saturation and degree of vacuum saturation, respectively, which is illustrated in Fig. 11 (red circle points for capillary saturation and red square points for vacuum saturation). There is a remarkable difference (with a factor of 5-10) in chloride diffusivity between capillary saturation and vacuum saturation. Moreover, due to EDL effect, the indirect methods for measuring the chloride diffusivity of cementitious materials, e.g. electrical resistivity method, may not provide accurate results. Olsson et al. [9] and Zhang et al. [12] both used the electrical resistivity method to explore the effect of w/c ratio on relative chloride diffusivity in non-saturated Portland cement mortar but reached the apparently contradictory conclusions. No relation between relative chloride diffusivity and degree of water saturation was observed by Olsson et al. [9], while Zhang et al. [12] concluded that the decrease of w/c ratio can lead to a significant reduction in relative chloride diffusivity at a given non-saturated state. For electrical resistivity tests, the attributes of pore solution of cementitious materials are usually assumed to be the same as those in free water (bulk solution), regardless of the pore structure of cementitious materials. Such assumption makes sense for the cementitious materials samples at a high water saturation level as the chloride conduction is dominantly governed by the water-filled larger pores and thus would be less affected by the EDL effect [14]. However, when the water saturation level reaches a low value, the water-filled smaller pores become the main diffusion paths for ions. Due to the significant EDL effect of water-filled smaller pores, the actual conductivity in pore solution of cementitious materials at a low water saturation level is lower than the calculated one considering the chloride concentration of pore solution [26, 59]. Therefore, the measured relative chloride diffusivity in non-saturated cementitious materials at a low water saturation level may have a deviation from the actual one. Besides, the measured relative chloride diffusivity is influenced by the testing cementitious samples. As seen in the purple points in Fig. 11, the relative chloride diffusivity in cement paste is consistently lower than that in concrete at a given degree of water saturation, especially at the sharp drop stage, which can be attributed to the presence of interfacial transition zone [77]. The attributes of raw materials, curing age of specimens, and sample pre-conditioning used in literature would not be identical to that for simulations in this study, which would inevitably result in a discrepancy between simulation results and experimental data, as the microstructure of cement paste is greatly affected by the raw materials, curing conditions and sample pre-conditioning [81].

In regard to modelling, the simulated microstructure of hierarchical cement paste cannot completely represent the realistic one, which may affect the accuracy of simulated chloride diffusivity. For instance, at the C-S-H level, apart from the colloidal model used in this study, disk-based packing model [82] and sheet-based model [83] were also developed to simulate the microstructure of C-S-H. However, since the 3D tomography of C-S-H has not been experimentally observed, the structure of C-S-H at nano-scale is still uncertain. At the cement paste level, the microstructure of cement paste

was simulated using the CEMHYD3D model with a resolution of 1 μm/voxel, where the capillary pores ≤ 1 μm cannot be covered although the majority of capillary pores are smaller than this resolution. As shown in Fig. 4, considering the realistic size of capillary pores, the chloride diffusivity in capillary pore solution is definitely influenced by the EDL effect and thus is much smaller than that in free water, which suggests that the simulated chloride diffusivity in cement paste in this study would be overestimated. Nevertheless, the coarser resolution can lead to a decrease in the connectivity of capillary pores in cement paste with the same porosity [38], as a result of which the simulated chloride diffusivity would be reduced. The modelling framework based on the generated microstructure from CEMHYD3D may offset the limitations of not considering the effect of EDL on small capillary pore solution due to limited resolution to a certain extent. In future work, a higher resolution can be adopted to simulate the 3D microstructure of cement paste with the use of improved computer configurations and computational efficiency and thus the EDL effect on chloride diffusion in pores at different length scales can be considered [84].

6. Conclusions

In this study, an integrated modelling framework was developed to simulate the distribution of water and gas phases and chloride diffusivity in non-saturated cement paste with various w/c ratios and saturation levels considering the contributions of capillary pores as well as gel pores in C-S-H. Based on the simulation results in comparison with experimental data obtained from literature, the main conclusions can be drawn as follows:

- The chloride diffusivity in pore solution is dependent on the surface electric potential, chloride concentration of bulk solution, and pore size. However, the effect of electrical double layer (EDL) on chloride diffusivity can be neglected when the pore size is ≥ 1 μm. Due to the small range of pore size between 1 nm and 6 nm, the chloride diffusivity in C-S-H pore solution is dominantly influenced by the surface electric potential. The simulated chloride diffusivity in C-S-H pore solution is 2.03×10^{-10} m²/s, which is close to 1.07×10^{-10} m²/s derived from the inversion analysis of the measured chloride diffusivity in cement paste.

- The relative chloride diffusivity in C-S-H is decreased with the decrease of degree of water saturation. The depercolation of non-saturated C-S-Hs with porosities of 19% and 28% occurs at a critical degree of water saturation of 24% and 21%, respectively, corresponding to a zero chloride diffusivity. The changing tendency of relative chloride diffusivity in non-saturated C-S-H shows a good correlation with the effective water-filled porosity of C-S-H gel against degree of water saturation.

- The chloride diffusivity in cement paste has a strong dependence on the degree of water saturation. The evolution of relative chloride diffusivity in cement paste with the decrease of water saturation follows four stages, i.e., a sharp drop stage, a slow decrease stage, a slight decrease stage and a

non-diffusive stage, where the connected water-filled capillary pores, the disconnected water-filled capillary pores and connected water-filled gel pores in C-S-H, and the connected water-filled gel pores in C-S-H act as the dominant diffusion channels, as well as the depercolation of pore network, respectively.

- The relative chloride diffusivity in cement paste with a higher w/c ratio at the sharp drop stage is more sensitive to the decreasing water saturation degree compared to the slow and slight decrease stages, as the water-filled capillary pore network is the dominant channel for chloride diffusion, which plays a more significant role in chloride diffusivity in cement paste with a higher w/c ratio. The relative chloride diffusivity in cement paste increases with decreasing w/c ratio at a given water saturation level. The simulated chloride diffusivity in non-saturated cement paste shows fairly good agreement with the experimental data obtained from literature in terms of change trend.

- It should be mentioned that chloride binding can lead to change in microstructure of cementitious materials as well as chloride diffusivity. Thus, it is vital to consider chloride binding in modelling of chloride diffusivity in cementitious materials, which was not addressed in this study but will be presented in future publications.

Table 1 Summary of experimental studies on chloride diffusivity in non-saturated cementitious materials.

Ref.	Binder	Specimen	w/c ratio	Paste porosity	Sample preconditioning	Test
Nielsen and Geiker [6]	PC	Mortar	0.5	–	Conditioned to 65% and 85% RH until constant weight	Natural diffusion
de Vera et al. [7]	CEM II/A-L 32.5	Concrete	0.6	0.50	Conditioned to 54%, 75%, 86% and >95% RH until constant weight	Natural diffusion
Olsson et al. [9]	CEM I 42.5N	Mortar	0.38, 0.53	0.39, 0.44	Conditioned to 33%, 59%, 75%, 85%, 91%, 94%, 97.5% and 100% RH until constant weight	Electrical resistivity
Mercado-Mendoza et al. [77]	CEM I	Paste, Concrete	0.43	0.39	Conditioned to 33%, 44%, 55%, 66%, 75%, 84% and 94% RH until constant weight	Electrical resistivity
Zhang et al. [12]	CEM I 42.5N	Mortar	0.4, 0.5, 0.6	0.155, 0.21, 0.277	Dried to target degree of water saturation	Electrical resistivity

References

[1] C. Liu, M. Zhang, Multiscale modelling of ionic diffusivity in unsaturated concrete accounting for its hierarchical microstructure, Cement and Concrete Research, 156 (2022) 106766.

[2] R.A. Patel, Q.T. Phung, S.C. Seetharam, J. Perko, D. Jacques, N. Maes, G. De Schutter, G. Ye, K. Van Breugel, Diffusivity of saturated ordinary Portland cement-based materials: A critical review of experimental and analytical modelling approaches, Cement and Concrete Research, 90 (2016) 52-72.

[3] Y. Zhang, M. Zhang, Transport properties in unsaturated cement-based materials–A review, Construction and Building Materials, 72 (2014) 367-379.

[4] M. Climent, G. De Vera, J. López, C. García, C. Andrade, Transport of chlorides through non-saturated concrete after an initial limited chloride supply, 2nd International RILEM Workshop on "Testing and Modelling the Chloride Ingress into Concrete", Paris, 2000.

[5] M.A. Climent, G. de Vera, J.F. López, E. Viqueira, C. Andrade, A test method for measuring chloride diffusion coefficients through nonsaturated concrete: Part I. The instantaneous plane source diffusion case, Cement and concrete Research, 32 (2002) 1113-1123.

[6] E.P. Nielsen, M.R. Geiker, Chloride diffusion in partially saturated cementitious material, Cement and Concrete Research, 33 (2003) 133-138.

[7] G. de Vera, M.A. Climent, E. Viqueira, C. Antón, C. Andrade, A test method for measuring chloride diffusion coefficients through partially saturated concrete. Part II: The instantaneous plane source diffusion case with chloride binding consideration, Cement and Concrete Research, 37 (2007) 714-724.

[8] A.T.d.C. Guimarães, M.A. Climent, G. De Vera, F.J. Vicente, F.T. Rodrigues, C. Andrade, Determination of chloride diffusivity through partially saturated Portland cement concrete by a simplified procedure, Construction and Building Materials, 25 (2011) 785-790.

[9] N. Olsson, V. Baroghel-Bouny, L.-O. Nilsson, M. Thiery, Non-saturated ion diffusion in concrete–A new approach to evaluate conductivity measurements, Cement and Concrete Composites, 40 (2013) 40-47.

[10] N. Olsson, B. Lothenbach, V. Baroghel-Bouny, L.-O. Nilsson, Unsaturated ion diffusion in cementitious materials–The effect of slag and silica fume, Cement and Concrete Research, 108 (2018) 31-37.

[11] Y. Zhang, M. Zhang, G. Ye, Influence of moisture condition on chloride diffusion in partially saturated ordinary Portland cement mortar, Materials and Structures, 51 (2018) 36.

[12] Y. Zhang, Z. Yang, G. Ye, Dependence of unsaturated chloride diffusion on the pore structure in cementitious materials, Cement and Concrete Research, 127 (2020) 105919.

[13] Y. Yang, M. Wang, Pore-scale modeling of chloride ion diffusion in cement microstructures,

Cement and Concrete Composites, 85 (2018) 92-104.

[14] H. Friedmann, O. Amiri, A. Aït-Mokhtar, Physical modeling of the electrical double layer effects on multispecies ions transport in cement-based materials, Cement and Concrete Research, 38 (2008) 1394-1400.

[15] A.V. Saetta, R.V. Scotta, R.V. Vitaliani, Analysis of chloride diffusion into partially saturated concrete, Materials Journal, 90 (1993) 441-451.

[16] V. Baroghel-Bouny, M. Thiéry, X. Wang, Modelling of isothermal coupled moisture–ion transport in cementitious materials, Cement and Concrete Research, 41 (2011) 828-841.

[17] Y. Zhang, G. Ye, A model for predicting the relative chloride diffusion coefficient in unsaturated cementitious materials, Cement and Concrete Research, 115 (2019) 133-144.

[18] S. Diamond, Mercury porosimetry: an inappropriate method for the measurement of pore size distributions in cement-based materials, Cement and Concrete Research, 30 (2000) 1517-1525.

[19] M. Zhang, G. Ye, K. van Breugel, Modeling of ionic diffusivity in non-saturated cement-based materials using lattice Boltzmann method, Cement and Concrete Research, 42 (2012) 1524-1533.

[20] K. Van Breugel, Numerical simulation of hydration and microstructural development in hardening cement-based materials (I) theory, Cement and Concrete Research, 25 (1995) 319-331.

[21] D. Hou, Y. Jia, J. Yu, P. Wang, Q. Liu, Transport properties of sulfate and chloride ions confined between calcium silicate hydrate surfaces: a molecular dynamics study, The Journal of Physical Chemistry C, 122 (2018) 28021-28032.

[22] P.J. McDonald, V. Rodin, A. Valori, Characterisation of intra-and inter-C-S-H gel pore water in white cement based on an analysis of NMR signal amplitudes as a function of water content, Cement and Concrete Research, 40 (2010) 1656-1663.

[23] R.A. Patel, J. Perko, D. Jacques, G. De Schutter, G. Ye, K. Van Bruegel, Effective diffusivity of cement pastes from virtual microstructures: Role of gel porosity and capillary pore percolation, Construction and Building Materials, 165 (2018) 833-845.

[24] F.-J. Ulm, G. Constantinides, F. Heukamp, Is concrete a poromechanics materials?—A multiscale investigation of poroelastic properties, Materials and Structures, 37 (2004) 43-58.

[25] M. Hlobil, V. Šmilauer, G. Chanvillard, Micromechanical multiscale fracture model for compressive strength of blended cement pastes, Cement and Concrete Research, 83 (2016) 188-202.

[26] C. Liu, Z. Liu, Y. Zhang, A multi-scale framework for modelling effective gas diffusivity in dry cement paste: Combined effects of surface, Knudsen and molecular diffusion, Cement and Concrete Research, 131 (2020) 106035.

[27] H.M. Jennings, A model for the microstructure of calcium silicate hydrate in cement paste, Cement and Concrete Research, 30 (2000) 101-116.

[28] A. Nonat, The structure and stoichiometry of CSH, Cement and Concrete Research, 34 (2004)

1521-1528.

[29] D.P. Bentz, D.A. Quenard, V. Baroghel-Bouny, E.J. Garboczi, H.M. Jennings, Modelling drying shrinkage of cement paste and mortar Part 1. Structural models from nanometres to millimetres, Materials and Structures, 28 (1995) 450-458.

[30] T.C. Powers, Structure and physical properties of hardened Portland cement paste, Journal of the American Ceramic Society, 41 (1958) 1-6.

[31] J. Yajun, J. Cahyadi, Simulation of silica fume blended cement hydration, Materials and Structures, 37 (2004) 397-404.

[32] L. Liu, X. Wang, H. Chen, C. Wan, M. Zhang, Numerical modeling of drying shrinkage deformation of cement-based composites by coupling multiscale structure model with 3D lattice analyses, Computers & Structures, 178 (2017) 88-104.

[33] S. Babaei, S. Seetharam, U. Muehlich, A. Dizier, G. Steenackers, B. Craeye, A multiscale framework to estimate water sorption isotherms for OPC-based materials, Cement and Concrete Composites, 105 (2020) 103415.

[34] B. Münch, L. Holzer, Contradicting geometrical concepts in pore size analysis attained with electron microscopy and mercury intrusion, Journal of the American Ceramic Society, 91 (2008) 4059-4067.

[35] R.F. Feldman, P.J. Sereda, A model for hydrated Portland cement paste as deduced from sorption-length change and mechanical properties, Matériaux et Construction, 1 (1968) 509-520.

[36] C. Liu, F. Wang, M. Zhang, Modelling of 3D microstructure and effective diffusivity of fly ash blended cement paste, Cement and Concrete Composites, (2020) 103586.

[37] C. Liu, R. Huang, Y. Zhang, Z. Liu, M. Zhang, Modelling of irregular-shaped cement particles and microstructural development of Portland cement, Construction and Building Materials, 168 (2018) 362-378.

[38] E.J. Garboczi, D.P. Bentz, The effect of statistical fluctuation, finite size error, and digital resolution on the phase percolation and transport properties of the NIST cement hydration model, Cement and Concrete Research, 31 (2001) 1501-1514.

[39] M. Zhang, G. Ye, K. Van Breugel, A numerical-statistical approach to determining the representative elementary volume (REV) of cement paste for measuring diffusivity, Materiales de Construcción, 60 (2010) 7-20.

[40] C. Liu, C. Qian, R. Qian, Z. Liu, H. Qiao, Y. Zhang, Numerical prediction of effective diffusivity in hardened cement paste between aggregates using different shapes of cement powder, Construction and Building Materials, 223 (2019) 806-816.

[41] A.K. Gunstensen, D.H. Rothman, S. Zaleski, G. Zanetti, Lattice Boltzmann model of immiscible fluids, Physical Review A, 43 (1991) 4320.

[42] M.R. Swift, W. Osborn, J. Yeomans, Lattice Boltzmann simulation of nonideal fluids, Physical Review Letters, 75 (1995) 830.

[43] X. He, S. Chen, R. Zhang, A lattice Boltzmann scheme for incompressible multiphase flow and its application in simulation of Rayleigh–Taylor instability, Journal of Computational Physics, 152 (1999) 642-663.

[44] T. Lee, C.-L. Lin, A stable discretization of the lattice Boltzmann equation for simulation of incompressible two-phase flows at high density ratio, Journal of Computational Physics, 206 (2005) 16-47.

[45] X. Shan, H. Chen, Lattice Boltzmann model for simulating flows with multiple phases and components, Physical Review E, 47 (1993) 1815.

[46] X. Shan, H. Chen, Simulation of nonideal gases and liquid-gas phase transitions by the lattice Boltzmann equation, Physical Review E, 49 (1994) 2941.

[47] P. Yuan, L. Schaefer, Equations of state in a lattice Boltzmann model, Physics of Fluids, 18 (2006) 042101.

[48] P. Lura, O.M. Jensen, K. Van Breugel, Autogenous shrinkage in high-performance cement paste: An evaluation of basic mechanisms, Cement and Concrete Research, 33 (2003) 223-232.

[49] Y.K. Suh, J. Kang, S. Kang, Assessment of algorithms for the no‑slip boundary condition in the lattice Boltzmann equation of BGK model, International Journal for Numerical Methods in Fluids, 58 (2008) 1353-1378.

[50] N. Jeong, D.H. Choi, C.-L. Lin, Estimation of thermal and mass diffusivity in a porous medium of complex structure using a lattice Boltzmann method, International Journal of Heat and Mass Transfer, 51 (2008) 3913-3923.

[51] X. He, Q. Zou, L.-S. Luo, M. Dembo, Analytic solutions of simple flows and analysis of nonslip boundary conditions for the lattice Boltzmann BGK model, Journal of Statistical Physics, 87 (1997) 115-136.

[52] I. Pointeau, P. Reiller, N. Macé, C. Landesman, N. Coreau, Measurement and modeling of the surface potential evolution of hydrated cement pastes as a function of degradation, Journal of Colloid and Interface Science, 300 (2006) 33-44.

[53] Y. Zhang, C. Liu, Z. Liu, G. Liu, L. Yang, Modelling of diffusion behavior of ions in low-density and high-density calcium silicate hydrate, Construction and Building Materials, 155 (2017) 965-980.

[54] A.W. Adamson, A.P. Gast, Physical Chemistry of Surfaces, 1997.

[55] O. Amiri, A. Aıt-Mokhtar, P. Dumargue, G. Touchard, Electrochemical modelling of chlorides migration in cement based materials. Part II: Experimental study-calculation of chlorides flux, Electrochimica Acta, 46 (2001) 3589-3597.

[56] F. He, C. Shi, X. Hu, R. Wang, Z. Shi, Q. Li, P. Li, X. An, Calculation of chloride ion

concentration in expressed pore solution of cement-based materials exposed to a chloride salt solution, Cement and Concrete Research, 89 (2016) 168-176.

[57] D. Hou, Z. Li, Molecular dynamics study of water and ions transported during the nanopore calcium silicate phase: case study of jennite, Journal of Materials in Civil Engineering, 26 (2014) 930-940.

[58] Y. Zhou, D. Hou, J. Jiang, P. Wang, Chloride ions transport and adsorption in the nano-pores of silicate calcium hydrate: experimental and molecular dynamics studies, Construction and Building Materials, 126 (2016) 991-1001.

[59] Y. Yang, R.A. Patel, S.V. Churakov, N.I. Prasianakis, G. Kosakowski, M. Wang, Multiscale modeling of ion diffusion in cement paste: electrical double layer effects, Cement and Concrete Composites, 96 (2019) 55-65.

[60] Z.C. Grasley, D.A. Lange, Thermal dilation and internal relative humidity of hardened cement paste, Materials and Structures, 40 (2007) 311-317.

[61] I. Maruyama, Y. Nishioka, G. Igarashi, K. Matsui, Microstructural and bulk property changes in hardened cement paste during the first drying process, Cement and Concrete Research, 58 (2014) 20-34.

[62] C. Zhou, F. Ren, Z. Wang, W. Chen, W. Wang, Why permeability to water is anomalously lower than that to many other fluids for cement-based material?, Cement and Concrete Research, 100 (2017) 373-384.

[63] C. Zhou, F. Ren, Q. Zeng, L. Xiao, W. Wang, Pore-size resolved water vapor adsorption kinetics of white cement mortars as viewed from proton NMR relaxation, Cement and Concrete Research, 105 (2018) 31-43.

[64] N.M. Alderete, Y.V. Zaccardi, N. De Belie, Physical evidence of swelling as the cause of anomalous capillary water uptake by cementitious materials, Cement and Concrete Research, 120 (2019) 256-266.

[65] H. Yu, X. Chen, Z. Wang, D. Deep, E. Lima, Y. Zhao, S.D. Teague, Mass-conserved volumetric lattice Boltzmann method for complex flows with willfully moving boundaries, Physical Review E, 89 (2014) 063304.

[66] D. Lowke, C. Gehlen, The zeta potential of cement and additions in cementitious suspensions with high solid fraction, Cement and Concrete Research, 95 (2017) 195-204.

[67] J. Plank, C. Hirsch, Impact of zeta potential of early cement hydration phases on superplasticizer adsorption, Cement and Concrete Research, 37 (2007) 537-542.

[68] H. Viallis-Terrisse, A. Nonat, J.-C. Petit, Zeta-potential study of calcium silicate hydrates interacting with alkaline cations, Journal of Colloid and Interface Science, 244 (2001) 58-65.

[69] L. Nachbaur, P.-C. Nkinamubanzi, A. Nonat, J.-C. Mutin, Electrokinetic properties which

control the coagulation of silicate cement suspensions during early age hydration, Journal of Colloid and Interface Science, 202 (1998) 261-268.

[70] P. Pivonka, C. Hellmich, D. Smith, Microscopic effects on chloride diffusivity of cement pastes—a scale-transition analysis, Cement and Concrete Research, 34 (2004) 2251-2260.

[71] K. Li, M. Stroeven, P. Stroeven, L.J. Sluys, Investigation of liquid water and gas permeability of partially saturated cement paste by DEM approach, Cement and Concrete Research, 83 (2016) 104-113.

[72] C. Liu, G. Liu, Z. Liu, L. Yang, M. Zhang, Y. Zhang, Numerical simulation of the effect of cement particle shapes on capillary pore structures in hardened cement pastes, Construction and Building Materials, 173 (2018) 615-628.

[73] M. Zhang, K. Xu, Y. He, A.P. Jivkov, Pore-scale modelling of 3D moisture distribution and critical saturation in cementitious materials, Construction and Building Materials, 64 (2014) 222-230.

[74] E. Garboczi, D. Bentz, Computer simulation of the diffusivity of cement-based materials, Journal of Materials Science, 27 (1992) 2083-2092.

[75] Q. Zeng, K. Li, T. Fen-Chong, P. Dangla, Pore structure characterization of cement pastes blended with high-volume fly-ash, Cement and Concrete Research, 42 (2012) 194-204.

[76] K. Kurumisawa, K. Tanaka, Three-dimensional visualization of pore structure in hardened cement paste by the gallium intrusion technique, Cement and Concrete Research, 36 (2006) 330-336.

[77] H. Mercado-Mendoza, S. Lorente, X. Bourbon, Ionic aqueous diffusion through unsaturated cementitious materials–A comparative study, Construction and Building Materials, 51 (2014) 1-8.

[78] A. Buchwald, Determination of the ion diffusion coefficient in moisture and salt loaded masonry materials by impedance spectroscopy, 3rd International PhD Symposium, 2000.

[79] C. Zhou, W. Chen, W. Wang, F. Skoczylas, Unified determination of relative molecular diffusivity and fluid permeability for partially saturated cement-based materials, Cement and Concrete Research, 67 (2015) 300-309.

[80] H.M. Jennings, A. Kumar, G. Sant, Quantitative discrimination of the nano-pore-structure of cement paste during drying: New insights from water sorption isotherms, Cement and Concrete Research, 76 (2015) 27-36.

[81] H.Y. Moon, H.S. Kim, D.S. Choi, Relationship between average pore diameter and chloride diffusivity in various concretes, Construction and Building Materials, 20 (2006) 725-732.

[82] Z. Yu, A. Zhou, D. Lau, Mesoscopic packing of disk-like building blocks in calcium silicate hydrate, Scientific Reports, 6 (2016) 36967.

[83] M.A. Etzold, P.J. McDonald, A.F. Routh, Growth of sheets in 3D confinements—a model for the C–S–H meso structure, Cement and Concrete Research, 63 (2014) 137-142.

[84] M. Zhang, Pore-scale modelling of relative permeability of cementitious materials using X-ray

computed microtomography images, Cement and Concrete Research, 95 (2017) 18-29.